Draft version January 10, 2024
Typeset using LaTeX twocolumn style in AASTeX631

Detection of X-ray Polarization from the Blazar 1ES 1959+650 with the Imaging X-ray Polarimetry Explorer

Manel Errando [1] Ioannis Liodakis [2,3] Alan P. Marscher [4] Herman L. Marshall [5] Riccardo Middei,[6,7] Michela Negro [8] Abel Lawrence Peirson [9] Matteo Perri [6,7] Simonetta Puccetti [6] Pazit L. Rabinowitz [1] Iván Agudo [10] Svetlana G. Jorstad [4,11] Sergey S. Savchenko,[11,12] Dmitry Blinov,[13,14] Ioakeim G. Bourbah,[14] Sebastian Kiehlmann [13,14] Evangelos Kontopodis,[14] Nikos Mandarakas [13,14] Stylianos Romanopoulos,[13,14] Raphael Skalidis,[13,14,15] Anna Vervelaki [14] Francisco José Aceituno,[10] Maria I. Bernardos,[10] Giacomo Bonnoli [16,10] Víctor Casanova,[10] Beatriz Agís-González,[10] César Husillos [10,17] Alessandro Marchini [18] Alfredo Sota [10] Pouya M. Kouch [2,19] Elina Lindfors,[2] Carolina Casadio,[13,14] Juan Escudero [20] Ioannis Myserlis [21,22] Ryo Imazawa,[23] Mahito Sasada,[24] Yasushi Fukazawa,[23,25,26] Koji S. Kawabata,[23,25,26] Makoto Uemura,[23,25,26] Tsunefumi Mizuno [25] Tatsuya Nakaoka,[25] Hiroshi Akitaya [27,25] Mark Gurwell [28] Garrett K. Keating [28] Ramprasad Rao,[28] Adam Ingram [29,30] Francesco Massaro [31,32] Lucio Angelo Antonelli [7,6] Raffaella Bonino [31,32] Elisabetta Cavazzuti [33] Chien-Ting Chen [34] Nicolò Cibrario [31,32] Stefano Ciprini [35,6] Alessandra De Rosa [36] Laura Di Gesu [33] Federico Di Pierro,[31] Immacolata Donnarumma [33] Steven R. Ehlert [3] Francesco Fenu,[37] Ephraim Gau [1] Vladimir Karas [38] Dawoon E. Kim [36,39,40] Henric Krawczynski [1] Marco Laurenti [35,6] Lindsey Lisalda [1] Rubén López-Coto,[20] Grzegorz Madejski,[9] Frédéric Marin [41] Andrea Marinucci [33] Ikuyuki Mitsuishi,[42] Fabio Muleri [36] Luigi Pacciani,[36] Alessandro Paggi,[32] Pierre-Olivier Petrucci [43] Nicole Rodriguez Cavero [1] Roger W. Romani [9] Fabrizio Tavecchio,[16] Stefano Tugliani [31,32] Kinwah Wu [44] Matteo Bachetti [45] Luca Baldini [46,47] Wayne H. Baumgartner [3] Ronaldo Bellazzini [46] Stefano Bianchi [48] Stephen D. Bongiorno [3] Alessandro Brez [46] Niccolò Bucciantini [49,50,51] Fiamma Capitanio [36] Simone Castellano [46] Enrico Costa [36] Ettore Del Monte [36] Niccolò Di Lalla [9] Alessandro Di Marco [36] Victor Doroshenko [52] Michal Dovčiak [38] Teruaki Enoto [53] Yuri Evangelista [36] Sergio Fabiani [36] Riccardo Ferrazzoli [36] Javier A. Garcia [54] Shuichi Gunji [55] Kiyoshi Hayashida,[56] Jeremy Heyl [57] Wataru Iwakiri [58] Philip Kaaret [3] Fabian Kislat [59] Takao Kitaguchi,[53] Jeffery J. Kolodziejczak [3] Fabio La Monaca [36,40,39] Luca Latronico [31] Simone Maldera [31] Alberto Manfreda [60] Giorgio Matt [48] C.-Y. Ng [61] Stephen L. O'Dell [3] Nicola Omodei [9] Chiara Oppedisano [31] Alessandro Papitto [7] George G. Pavlov [62] Melissa Pesce-Rollins [46] Maura Pilia [45] Andrea Possenti [45] Juri Poutanen [19] Brian D. Ramsey [3] John Rankin [36] Ajay Ratheesh [36] Oliver J. Roberts [34] Carmelo Sgrò [46] Patrick Slane [63] Paolo Soffitta [36] Gloria Spandre [46] Douglas A. Swartz [34] Toru Tamagawa [53] Fabrizio Tavecchio [16] Roberto Taverna [64] Yuzuru Tawara,[42] Allyn F. Tennant [3] Nicholas E. Thomas [3] Francesco Tombesi [40,35,65] Alessio Trois [45] Sergey S. Tsygankov [19] Roberto Turolla [64,44] Jacco Vink [66] Martin C. Weisskopf [3] Fei Xie [67,36] and Silvia Zane [44]

[1] Physics Department and McDonnell Center for the Space Sciences, Washington University in St. Louis, St. Louis, MO 63130, USA
[2] Finnish Centre for Astronomy with ESO, 20014 University of Turku, Finland
[3] NASA Marshall Space Flight Center, Huntsville, AL 35812, USA
[4] Institute for Astrophysical Research, Boston University, 725 Commonwealth Avenue, Boston, MA 02215, USA
[5] MIT Kavli Institute for Astrophysics and Space Research, Massachusetts Institute of Technology, 77 Massachusetts Avenue, Cambridge, MA 02139, USA
[6] Space Science Data Center, Agenzia Spaziale Italiana, Via del Politecnico snc, 00133 Roma, Italy
[7] INAF Osservatorio Astronomico di Roma, Via Frascati 33, 00078 Monte Porzio Catone (RM), Italy
[8] Department of Physics and Astronomy, Louisiana State University, Baton Rouge, LA 70803, USA
[9] Department of Physics and Kavli Institute for Particle Astrophysics and Cosmology, Stanford University, Stanford, California 94305, USA

Corresponding author: Manel Errando
errando@wustl.edu

[10]Instituto de Astrofísica de Andalucía - CSIC, Glorieta de la Astronomía s/n, 18008, Granada, Spain
[11]Saint Petersburg State University, 7/9 Universitetskaya nab., St. Petersburg, 199034 Russia
[12]Pulkovo Observatory, St.Petersburg, 196140, Russia
[13]Institute of Astrophysics, Foundation for Research and Technology-Hellas, GR-70013 Heraklion, Greece
[14]Department of Physics, University of Crete, 70013, Heraklion, Greece
[15]Owens Valley Radio Observatory, California Institute of Technology, MC 249-17, Pasadena, CA 91125, USA
[16]INAF Osservatorio Astronomico di Brera, Via E. Bianchi 46, 23807 Merate (LC), Italy
[17]Geological and Mining Institute of Spain (IGME-CSIC), Calle Ríos Rosas 23, E-28003, Madrid, Spain
[18]University of Siena, Astronomical Observatory, Via Roma 56, 53100 Siena, Italy
[19]Department of Physics and Astronomy, 20014 University of Turku, Finland
[20]Instituto de Astrofísica de Andalucía-CSIC, Glorieta de la Astronomía s/n, 18008, Granada, Spain
[21]Institut de Radioastronomie Millimétrique, Avenida Divina Pastora, 7, Local 20, E–18012 Granada, Spain
[22]Max-Planck-Institut für Radioastronomie, Auf dem Hügel 69, D-53121 Bonn, Germany
[23]Department of Physics, Graduate School of Advanced Science and Engineering, Hiroshima University, Kagamiyama, 1-3-1 Higashi-Hiroshima, Hiroshima 739-8526, Japan
[24]Department of Physics, Tokyo Institute of Technology, 2-12-1 Ookayama, Meguro-ku, Tokyo 152-8551, Japan
[25]Hiroshima Astrophysical Science Center, Hiroshima University, 1-3-1 Kagamiyama, Higashi-Hiroshima, Hiroshima 739-8526, Japan
[26]Core Research for Energetic Universe (Core-U), Hiroshima University, 1-3-1 Kagamiyama, Higashi-Hiroshima, Hiroshima 739-8526, Japan
[27]Planetary Exploration Research Center, Chiba Institute of Technology, 2-17-1 Tsudanuma, Narashino 275-0016, Japan
[28]Center for Astrophysics — Harvard & Smithsonian, 60 Garden Street, Cambridge, MA 02138 USA
[29]Department of Physics – Astrophysics, University of Oxford, Denys Wilkinson Building, Keble Road, Oxford OX1 3RH, UK
[30]School of Mathematics, Statistics and Physics, Newcastle University, Herschel Building, Newcastle upon Tyne, NE1 7RU, UK
[31]Istituto Nazionale di Fisica Nucleare, Sezione di Torino, Via Pietro Giuria 1, 10125 Torino, Italy
[32]Dipartimento di Fisica, Università degli Studi di Torino, Via Pietro Giuria 1, 10125 Torino, Italy
[33]ASI - Agenzia Spaziale Italiana, Via del Politecnico snc, 00133 Roma, Italy
[34]Science and Technology Institute, Universities Space Research Association, Huntsville, AL 35805, USA
[35]Istituto Nazionale di Fisica Nucleare, Sezione di Roma "Tor Vergata", Via della Ricerca Scientifica 1, 00133 Roma, Italy
[36]INAF Istituto di Astrofisica e Planetologia Spaziali, Via del Fosso del Cavaliere 100, 00133 Roma, Italy
[37]Karlsruhe Institute of Technology (KIT), Institute for Astroparticle Physics, Karlsruhe, Germany
[38]Astronomical Institute of the Czech Academy of Sciences, Boční II 1401/1, 14100 Praha 4, Czech Republic
[39]Dipartimento di Fisica, Università degli Studi di Roma "La Sapienza", Piazzale Aldo Moro 5, 00185 Roma, Italy
[40]Dipartimento di Fisica, Università degli Studi di Roma "Tor Vergata", Via della Ricerca Scientifica 1, 00133 Roma, Italy
[41]Université de Strasbourg, CNRS, Observatoire Astronomique de Strasbourg, UMR 7550, 67000 Strasbourg, France
[42]Graduate School of Science, Division of Particle and Astrophysical Science, Nagoya University, Furo-cho, Chikusa-ku, Nagoya, Aichi 464-8602, Japan
[43]Université Grenoble Alpes, CNRS, IPAG, 38000 Grenoble, France
[44]Mullard Space Science Laboratory, University College London, Holmbury St Mary, Dorking, Surrey RH5 6NT, UK
[45]INAF Osservatorio Astronomico di Cagliari, Via della Scienza 5, 09047 Selargius (CA), Italy
[46]Istituto Nazionale di Fisica Nucleare, Sezione di Pisa, Largo B. Pontecorvo 3, 56127 Pisa, Italy
[47]Dipartimento di Fisica, Università di Pisa, Largo B. Pontecorvo 3, 56127 Pisa, Italy
[48]Dipartimento di Matematica e Fisica, Università degli Studi Roma Tre, Via della Vasca Navale 84, 00146 Roma, Italy
[49]INAF Osservatorio Astrofisico di Arcetri, Largo Enrico Fermi 5, 50125 Firenze, Italy
[50]Dipartimento di Fisica e Astronomia, Università degli Studi di Firenze, Via Sansone 1, 50019 Sesto Fiorentino (FI), Italy
[51]Istituto Nazionale di Fisica Nucleare, Sezione di Firenze, Via Sansone 1, 50019 Sesto Fiorentino (FI), Italy
[52]Institut für Astronomie und Astrophysik, Universität Tübingen, Sand 1, 72076 Tübingen, Germany
[53]RIKEN Cluster for Pioneering Research, 2-1 Hirosawa, Wako, Saitama 351-0198, Japan
[54]NASA Goddard Space Flight Center, Greenbelt, MD 20771, USA
[55]Yamagata University,1-4-12 Kojirakawa-machi, Yamagata-shi 990-8560, Japan
[56]Osaka University, 1-1 Yamadaoka, Suita, Osaka 565-0871, Japan
[57]University of British Columbia, Vancouver, BC V6T 1Z4, Canada
[58]International Center for Hadron Astrophysics, Chiba University, Chiba 263-8522, Japan
[59]Department of Physics and Astronomy and Space Science Center, University of New Hampshire, Durham, NH 03824, USA
[60]Istituto Nazionale di Fisica Nucleare, Sezione di Napoli, Strada Comunale Cinthia, 80126 Napoli, Italy
[61]Department of Physics, The University of Hong Kong, Pokfulam, Hong Kong
[62]Department of Astronomy and Astrophysics, Pennsylvania State University, University Park, PA 16802, USA
[63]Center for Astrophysics — Harvard & Smithsonian, 60 Garden St, Cambridge, MA 02138, USA

[64] *Dipartimento di Fisica e Astronomia, Università degli Studi di Padova, Via Marzolo 8, 35131 Padova, Italy*
[65] *Department of Astronomy, University of Maryland, College Park, Maryland 20742, USA*
[66] *Anton Pannekoek Institute for Astronomy & GRAPPA, University of Amsterdam, Science Park 904, 1098 XH Amsterdam, The Netherlands*
[67] *Guangxi Key Laboratory for Relativistic Astrophysics, School of Physical Science and Technology, Guangxi University, Nanning 530004, China*

ABSTRACT

Observations of linear polarization in the 2-8 keV energy range with the Imaging X-ray Polarimetry Explorer (*IXPE*) explore the magnetic field geometry and dynamics of the regions generating non-thermal radiation in relativistic jets of blazars. These jets, particularly in blazars whose spectral energy distribution peaks at X-ray energies, emit X-rays via synchrotron radiation from high-energy particles within the jet. *IXPE* observations of the X-ray selected BL Lac-type blazar 1ES 1959+650 in 2022 May 3-4 showed a significant linear polarization degree of $\Pi_{\rm x} = 8.0\% \pm 2.3\%$ at an electric-vector position angle $\psi_{\rm x} = 123^{\circ} \pm 8^{\circ}$. However, in 2022 June 9-12, only an upper limit of $\Pi_{\rm x} \leq 5.1\%$ could be derived (at the 99% confidence level). The degree of optical polarization at that time $\Pi_{\rm O} \sim 5\%$ is comparable to the X-ray measurement. We investigate possible scenarios for these findings, including temporal and geometrical depolarization effects. Unlike some other X-ray selected BL Lac objects, there is no significant chromatic dependence of the measured polarization in 1ES 1959+650, and its low X-ray polarization may be attributed to turbulence in the jet flow with dynamical timescales shorter than 1 day.

Keywords: Relativistic jets (1390); X-ray active galactic nuclei (2035); Active galactic nuclei (16); Blazars (164); Spectropolarimetry (1973)

1. INTRODUCTION

Relativistic jets are powerful streams of collimated plasma and radiation that play a prominent role in various astrophysical phenomena, such as active galactic nuclei, gamma-ray bursts, and X-ray binary systems (Begelman et al. 1984; Falcke et al. 2004; Hughes & Bregman 2006; Blandford et al. 2019). In the case of blazars, these jets are fueled by accretion onto a central supermassive black hole within an active galactic nucleus, and are oriented in a direction that is closely aligned with Earth's line of sight (Urry & Padovani 1995). These jets accelerate particles to energies beyond 10^{10} eV, producing non-thermal emission observed across a wide range of frequencies, from radio to very high-energy (VHE, > 0.1 TeV) γ rays (Giommi et al. 2012; Liodakis et al. 2019). Advancements in understanding the physics of relativistic jets rely heavily on multi-wavelength observations encompassing the spectral energy distribution, flux variability, and polarization of the observed emission.

According to most theoretical models for the production, acceleration, and collimation of relativistic jets, the plasma is Poynting-flux dominated close to the black hole, where the jet is accelerated and collimated (e.g., Blandford & Znajek 1977; Vlahakis & Königl 2004). Near the end of the acceleration and collimation zone, there is a transition to a particle-dominated flow (e.g., Lyubarsky 2010). It is currently unclear, however, where most of the particle acceleration and radiative dissipation take place. Multiple processes could play major roles in energizing the particles that produce the radiation in blazar jets. These include magnetic reconnection events (e.g., Romanova & Lovelace 1992; Kagan et al. 2015; Werner et al. 2018), relativistic shocks (e.g., Blandford & Ostriker 1978; Nishikawa et al. 2003; Sironi et al. 2015a), and stochastic particle acceleration (e.g., Dermer et al. 1996; Kirk et al. 1996; Katarzyński et al. 2006). These mechanisms can efficiently accelerate particles, although particle-in-cell simulations find that magnetic reconnection is more efficient than shocks at doing so where the magnetization level is high (Sironi & Spitkovsky 2014). On the other hand, shocks can be more efficient in regions where the magnetization is low (Sironi et al. 2015b).

Multi-wavelength observations of linear polarization probe the geometry of the magnetic field in different locations in relativistic jets (e.g., Angel & Stockman 1980; Jorstad et al. 2005; Marscher & Jorstad 2021). The results can indicate which of the particle acceleration mechanisms are operating in sites of strong high-energy radiation (e.g., Zhang et al. 2019; Tavecchio 2021; Zhang et al. 2022; Di Gesu et al. 2022a; Marscher & Jorstad 2022). Such polarization observations of blazars have long been available at radio, infrared and optical wavelengths. Observations in the X-ray band now benefit from the availability of linear polarization sensitivity through the Imaging X-ray Polarimetry Explorer satellite (*IXPE*, Weisskopf et al. 2022), which began science operations on 2022 January 11. *IXPE* consists of three 4 m focal-length X-ray mirrors that focus on three identical polarization-sensitive gas pixel detector units (DU1-3). The sensitivity of an X-ray polarimeter is commonly assessed by its minimum detectable polarization at 99% confidence level, MDP_{99}. At a flux level of $F_{2-8\,\mathrm{keV}} = 10^{-10}\,\mathrm{erg\,cm^{-2}\,s^{-1}}$, *IXPE* achieves $MDP_{99} \approx 8\%$ in a 50 ks exposure.

The BL Lacertae object 1ES 1959+650 ($z = 0.047$, de Vaucouleurs et al. 1991) stands out as one of the brightest X-ray blazars. Only four BL Lac objects in the Einstein Slew Survey exhibit a higher X-ray flux (Perlman et al. 1996). It is also among the first blazars from which TeV γ rays have been detected (Holder et al. 2003). The X-ray flux of 1ES 1959+650 generally exceeds $10^{-10}\mathrm{erg\,cm^{-2}\,s^{-1}}$ in the 0.1-10 keV range, displaying variability on timescales < 1 h (Kapanadze et al. 2014). While X-ray and γ-ray fluxes are generally found to be correlated, a notable "orphan" TeV flare without an X-ray counterpart was detected by the Whipple observatory in 2002 (Krawczynski et al. 2004). Owing to its bright X-ray emission, 1ES 1959+650 was among the first blazars observed by *IXPE*.

The radio to X-ray emission from 1ES 1959+650 is commonly interpreted as originating from synchrotron radiation by relativistic electrons cooling in the jet's magnetic field. Synchrotron radiation is inherently polarized. The expected degree of polarization from a power-law energy spectrum of relativistic electrons $N(E_e) \propto E_e^{-s}$ in a homogeneous magnetic field is $\Pi = (s+1)/(s+7/3) \approx 70\%$ for $s \approx 2$ (Rybicki & Lightman 1979). If the magnetic field configuration has a random component B_r then the polarization degree will be suppressed by a factor $B_0^2/(B_0^2 + B_r^2)$, where B_0 is the intensity of the ordered magnetic field component (Ginzburg & Syrovatskii 1965). In blazars, the presence of a random component in the magnetic field reduces the polarization signal from a maximum value of order 75% to an average value that is usually between a few and tens of percent (e.g., Blinov et al. 2021; Marscher & Jorstad 2021). Therefore, polarization measurements in the X-ray band by *IXPE* are sensitive to the relative ratio of the random to the ordered magnetic field in the region of the jet where the non-thermal emission from the highest-energy particles is emitted. This new probe of the magnetic field intensity and geometry in relativistic jets can be used to discern among the possible models for particle acceleration. For instance, if acceleration occurs in stationary shocks, downstream of which particles lose energy, we anticipate steady X-ray emission with higher polarization than than the polarization of the optical emission by lower-energy particles radiating over a larger volume (Angelakis et al. 2016; Tavecchio et al. 2018, 2020; Zhang et al. 2022; Di Gesu et al. 2022a; Marscher & Jorstad 2022). Conversely, magnetic reconnection events convert magnetic energy into kinetic energy, resulting in moderate X-ray and optical polarization, with a weaker dependence on photon energy (e.g., Bodo et al. 2021; Zhang et al. 2022).

Here we present the first detection of linear X-ray polarization from 1ES 1959+650 by *IXPE* in 2022 May 3-4 and June 9-12. We describe the *IXPE* measurements, as well as X-ray spectral observations with the Neil Gehrels Swift X-ray Telescope (*Swift*-XRT) and *XMM-Newton* in §2, and observations at other wavebands in §3. We discuss and interpret the results in §4 and summarize our findings in §5.

2. X-RAY OBSERVATIONS

IXPE first observed 1ES 1959+650 on 2022 May 3-4 with an exposure time of 54 ks. A second science observation was carried out on 2022 June 9-12, accumulating 200 ks of exposure. *XMM-Newton* (Strüder et al. 2001) collected two contemporaneous exposures of 1ES 1959+650, and *Swift*-XRT (Burrows et al. 2005) monitored the source with a total of eleven exposures during the duration of campaign.

We combine the *IXPE* Stokes I, *Swift*-XRT, and *XMM-Newton* spectra to characterize the energy spectrum of 1ES 1959+650 in the X-ray band. The goal of this combined fit is to determine the column density absorption and spectral shape of the X-ray spectrum of 1ES 1959+650, as the 2-8 keV energy range of *IXPE* is too narrow to robustly measure the level of neutral density absorption and the potential presence of spectral curvature. The flux normalizations and spectral properties are left free to allow for inter-calibration uncertainties (Madsen et al. 2017) as well as flux and spectral variability on timescales of days, which is often observed in 1ES 1959+650 even in relatively quiescent X-ray states (Tagliaferri et al. 2008). The fit of the combined data set to an absorbed power law $dN/dE \propto E^{-\Gamma_\mathrm{x}}$ yields a χ^2/dof fit statistic of 554/497 (with associated probability $p = 0.04$) for the May 3-4 data and 616/566 ($p = 0.07$) for June 9-12 (Figure 1). The best-fit parameters describing the spectra are listed in Table 1. Changing the model to an absorbed log-parabola does not significantly improve the fit in either case. The derived column density of $(1.32 \pm 0.04) \times 10^{21}\,\mathrm{cm}^{-2}$, exceeding

Table 1. Summary and results from *IXPE*, *XMM-Newton*, and *Swift*-XRT X-ray observations in 2022 May 3-4 and June 9-12.

Telescope	Energy range [keV]	ObsID	Date	Exposure [ks]	$F_{2-8\,\mathrm{keV}}$ $[10^{-10}\,\mathrm{erg\,cm^{-2}\,s^{-1}}]$	Γ_x	χ^2/dof
2022 May 3-4							
IXPE	2.0-8.0	01006201	2022 05 03-04	54	1.24 ± 0.02	2.50 ± 0.02	30.6/26
Swift-XRT	0.5-10	00096560006	2022 05 03	0.9	1.57 ± 0.04	2.18 ± 0.04	314/349
Swift-XRT	0.5-10	00096560007	2022 05 04	0.9	1.63 ± 0.05	2.17 ± 0.04	374/351
XMM-Newton	1.0-10	0902110801	2022 05 06	16	1.35 ± 0.01	2.26 ± 0.01	196/155
2022 June 9-12							
IXPE	2.0-8.0	01006001	2022 06 09-12	200	1.47 ± 0.01	2.29 ± 0.01	36.5/25
Swift-XRT	0.5-10	00096560012	2022 06 12	0.9	2.23 ± 0.05	2.20 ± 0.04	334/344
XMM-Newton	1.0-10	0902111201	2022 06 23	18	1.34 ± 0.01	2.20 ± 0.01	195/155

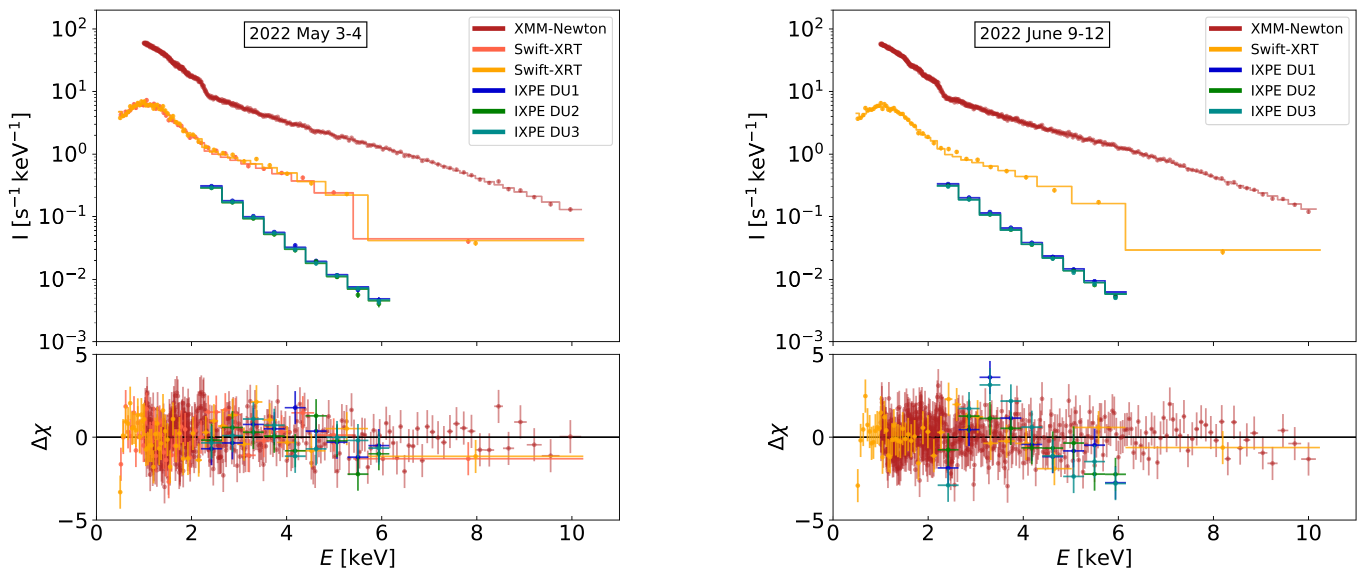

Figure 1. Spectral fit to the X-ray data of 1ES 1959+650 during *IXPE* observations in 2022 May 3-4 (*left panel*) and 2022 June 9-12 (*right panel*). The *IXPE* Stokes I, *Swift*-XRT, and *XMM-Newton* spectra are fit to derive the column density absorption and determine the presence of spectral curvature. These results will be used in the later spectro-polarimetric fit of the *IXPE* I, Q, and U spectra.

the Galactic value by 30% (HI4PI Collaboration et al. 2016), suggests the presence of additional neutral absorption along the line of sight within the host galaxy to the object, consistent with previous studies (Aliu et al. 2013, 2014). During both epochs, the average X-ray flux is within 10% of the median value measured by *Swift*-XRT between 2005 and 2022 (Figure 2; Stroh & Falcone 2013). We conclude that 1ES 1959+650 was in an average X-ray flux state during the *IXPE* campaign.

We have searched for time-averaged X-ray polarization from 1ES 1959+650 in the *IXPE* data. First the I spectra were fit with an absorbed power-law model. The absorbing column density was fixed to the value obtained during the combined spectral fit, but the powerlaw normalization and photon index were allowed to vary. We then tested for the presence of a constant degree of polarization and angle as a function of energy by performing a spectropolarimetric fit to the Stokes I, Q, and U spectra, with the only free parameters being the degree of polarization and polarization angle (Figure 3).

In May 3-4, the spectrum obtained from *IXPE* displayed a softer photon index of $\Gamma = 2.50 \pm 0.02$ compared to the contemporaneous *XMM-Newton* and *Swift*-XRT data (Table 1). In June 9-12 the *IXPE*-derived $\Gamma = 2.29 \pm 0.01$ was in closer agreement with the value previously derived. The effect is likely to be the result of an improvement in the telescope alignment between the two observations. The polarization degree in May 3-4 was $\Pi_\mathrm{x} = 8.0\% \pm 2.3\%$, with an electric-vector position angle $\psi_\mathrm{x} = 123° \pm 8°$. A null hypothesis of no linear

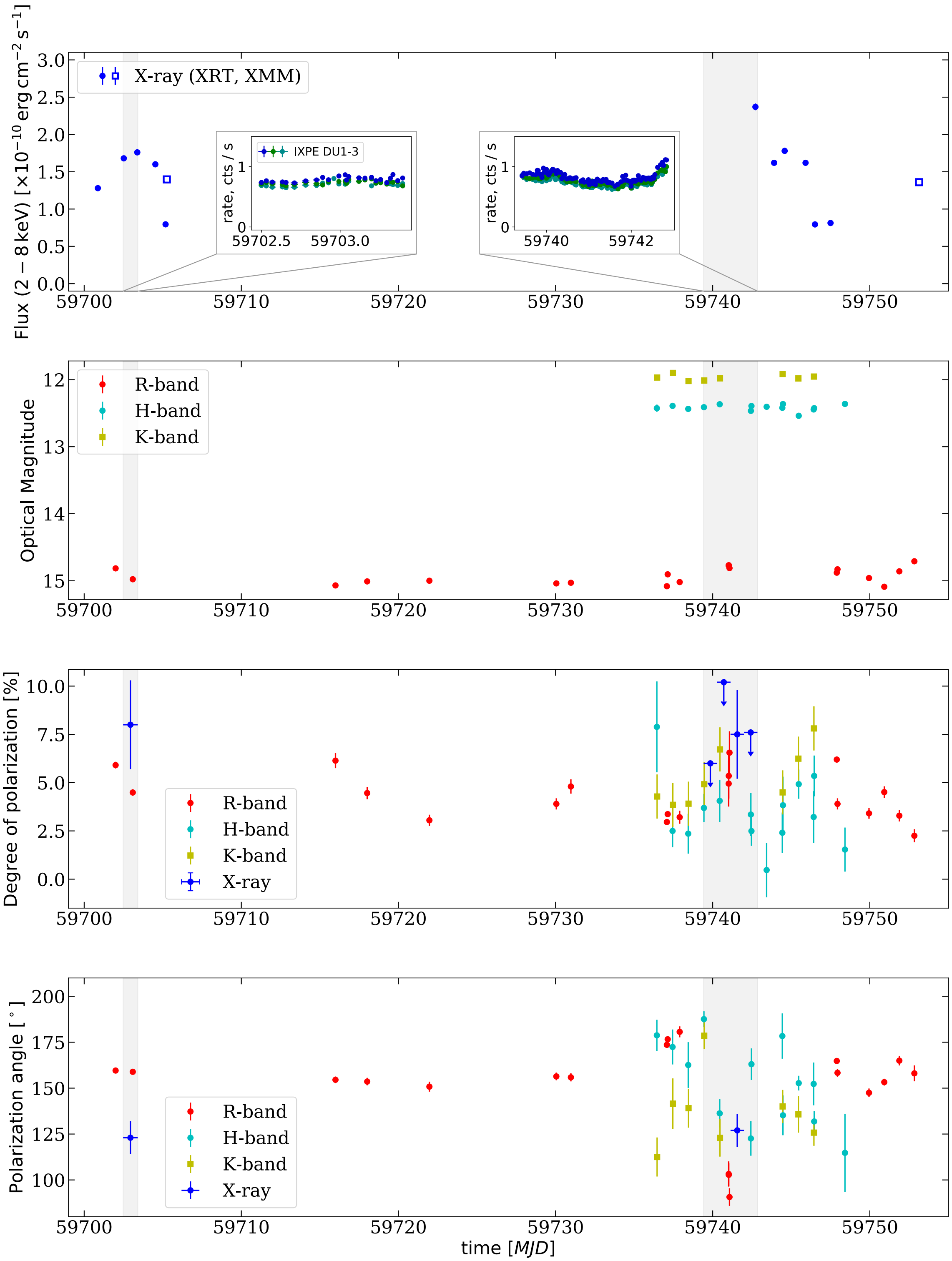

Figure 2. X-ray, optical, and IR light curves contemporaneous with the *IXPE* observations of 1ES 1959+650. Observations are described in §2 and §3. Panels show, from top to bottom, X-ray flux, optical and IR brightness in magnitudes, degree of polarization, and polarization angle. Inset plots in the top panel display the X-ray light curve measured by *IXPE*. Blue data points represent significant measurements of X-ray polarization, while blue downward-pointing arrows indicate 99% confidence level upper limits during time periods without a significant detection X-ray polarization. Grey vertical shaded areas indicate the two epochs of observation of *IXPE*.

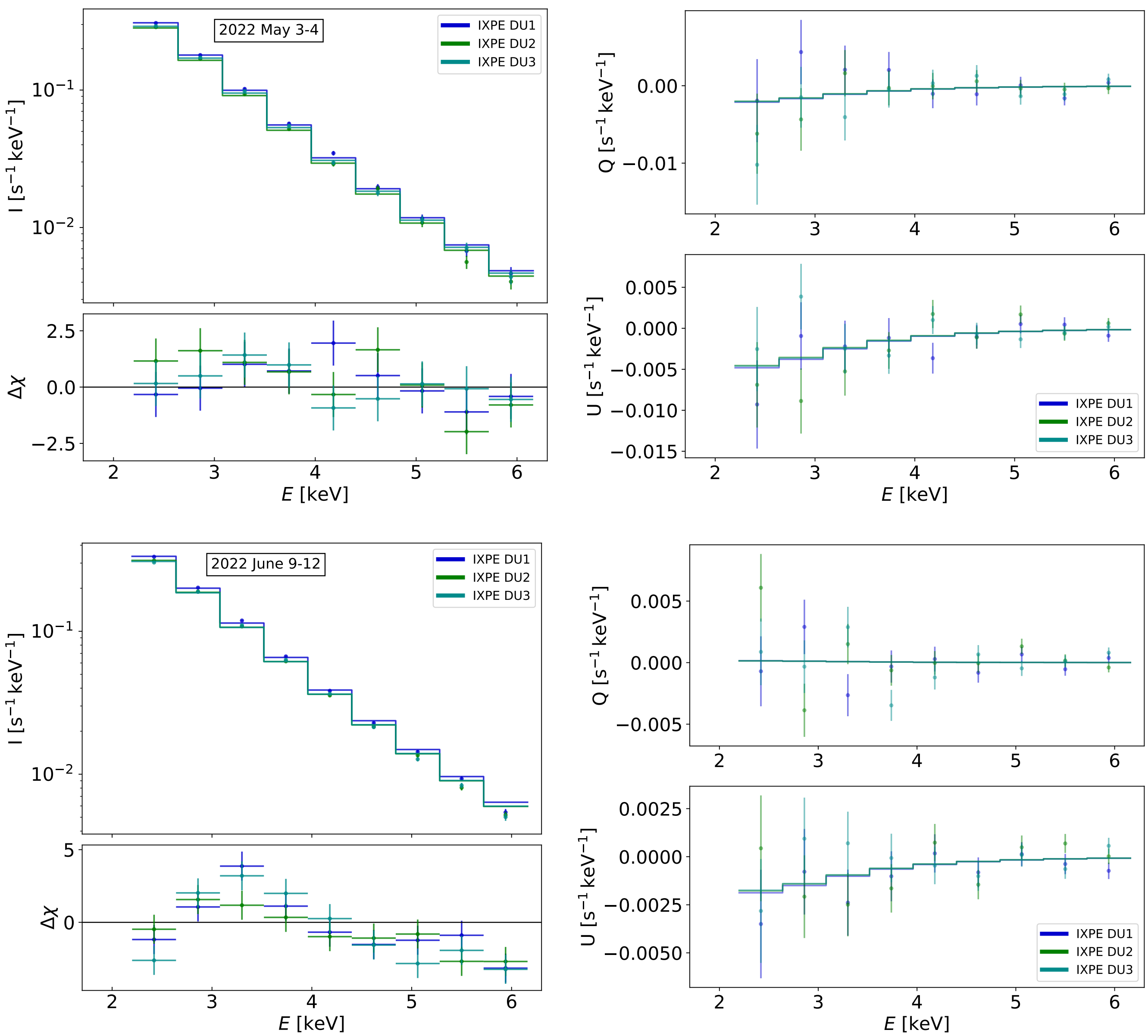

Figure 3. Spectro-polarimetric fit to the X-ray data of 1ES 1959+650 during *IXPE* observations in 2022 May 3-4 (*top panels*) and 2022 June 9-12 (*bottom panels*). Panels on the left present the fit to the *IXPE* Stokes I with its residuals, while panels on the right show the fits to the *IXPE* Q and U spectra.

polarization can be excluded at $3.5\,\sigma$ confidence level. No significant linear polarization was detected in June 9-12. From this second *IXPE* observation, we derive an upper limit of $\Pi_{\rm x} < 5.1\%$ (99% confidence level), with the polarization angle left unconstrained. The hypothesis that the degree of polarization remained constant across the May 3-4 and June 9-12 *IXPE* observations has an associated probability of $P = 0.0244$ using a χ^2 test, i.e. it can only be excluded at $2.3\,\sigma$ level.

To search for time-dependent X-ray polarization, we split the 200 ks-duration *IXPE* exposure from June 9-12 into four 50 ks slices and repeated the spectro-polarimetric fit described above independently for each time bin. We found no significant linear polarization in three out of the four segments, with only the third one showing significant polarization corresponding to a $2.8\,\sigma$ post-trial confidence level (Figure 2). The constraints on the degree of polarization in the four time bins are $\Pi_{\rm x} < 6.0\%$, $< 10.2\%$, $7.5\% \pm 2.3\%$, and $< 7.6\%$ (upper limits are 99% confidence level). The polarization angle is only constrained for the third time bin to be $\psi_{\rm x} = 127° \pm 9°$.

X-ray data reduction procedures are detailed in Appendix A.

3. RADIO, INFRARED, AND OPTICAL OBSERVATIONS

Figure 2 summarizes the time evolution on the X-ray and optical polarization measurements of 1ES 1959+650. Contemporaneous polarization observations were obtained at radio (millimeter), infrared (IR), and optical wavelengths using the Institut de Radioastronomie Millimétrique (IRAM) 30 m radio telescope, the 1.8 m Perkins Telescope, the Calar alto observatory, the KANATA telescope, the Nordic Optical Telescope (NOT), the Sierra Nevada Observatory, RoboPol mounted at the 1.3 m telescope of the Skinakas Observatory, the Submillimeter Array (SMA), and the Very Long Baseline Array (VLBA).

Images of 1ES 1959+650 obtained at 7 mm (43 GHz) from VLBA data feature a ~ 1 milliarcsecond jet extending to the southeast of a compact "core" along a position angle of $\phi \sim 150°$ (Piner et al. 2010; Weaver et al. 2022). Figure 4 presents VLBA images at three epochs near the *IXPE* pointings obtained as part of the BEAM-ME monitoring project[1]. The data were obtained and analyzed using standard procedures, as described by Jorstad et al. (2017). We measure the linear polarization of the core to be $P_{\rm core} = 2.3\% \pm 0.2\%$ along $\psi_{\rm core} = 173 \pm 10°$ on 2022 June 5, and $P_{\rm core} = 2.8\% \pm 0.3\%$ along $\psi_{\rm core} = 152 \pm 10°$ on 2022 June 24. We determine only an upper limit to the degree of polarization of $P_{\rm core} \leq 2.4\%$ on 2022 April 30. When the resolved 43 GHz emission is included, the degree of polarization decreases to $P = 1.5\% \pm 0.5\%$ and $P = 1.7\% \pm 0.9\%$ on June 5 and 24, respectively.

The IRAM observations were obtained during the first *IXPE* observation on 2022 May 5 (MJD 59705.0138) and during the second observation on 2022 June 12 (MJD 59742.9538) at 86.24 and 228.93 GHz, under the Polarimetric Monitoring of AGN at Millimeter Wavelengths (POLAMI) Large Program[2] (Agudo et al. 2018b,a; Thum et al. 2018). For the first observation, we obtained a 99% upper limit of $\Pi_{\rm R} < 8\%$ for the polarization degree at 228 GHz. During the second *IXPE* measurement, the IRAM observations yielded upper limits of $\Pi_{\rm R} < 1.6\%$ and $< 9.6\%$ at 86 GHz and 228 GHz, respectively.

SMA observations were obtained between the two IXPE exposures on 2022 June 1 (MJD 59731.60152) and 2022 June 6 (MJD 59736.71253) at 225.3 GHz within the SMAPOL (SMA Monitoring of AGNs with POLarization) program. Data were taken with the SMA polarimeter (Marrone & Rao 2008) in full polarization mode using the SWARM correlator (Primiani et al. 2016). MWC 349 A, and Callisto were used as the total flux calibrators and 3C 286 as the polarization calibrator. We find a low degree of polarization $\Pi_{\rm R} = 1.92 \pm 0.58\%$ along $\psi_{\rm R} = 129° \pm 8°$ for the first observation, and $\Pi_{\rm R} = 2.53 \pm 0.5\%$ along $\psi_{\rm R} = 156° \pm 5°$ for the second one.

IR photometric and polarimetric data in H ($1.6\,\mu$m) and K ($2.2\,\mu$m) bands during the June 9-12 *IXPE* exposures were obtained using the MIMIR camera[3] at the Perkins Telescope (PTO, Flagstaff, AZ), operated by Boston University. The average and standard deviation of the host-corrected IR polarization degree was found to be $\Pi_{\rm H} = 3.27\% \pm 0.16\%$ along a polarization angle $\psi_{\rm H} = 162° \pm 25°$ and $\Pi_{\rm K} = 4.73\% \pm 0.75\%$ along $\psi_{\rm K} = 151° \pm 28°$.

During the first *IXPE* observation, we only have a single optical measurement from NOT, which yielded an optical polarization degree $\Pi_{\rm O} = 4.49 \pm 0.17\%$ along $\psi_{\rm O} = 159 \pm 1°$. During the second *IXPE* observation, the median and standard deviation of the optical polarization degree was $\Pi_{\rm O} = 5.4\% \pm 1.1\%$ along $\psi_{\rm O} = 103° \pm 6°$. The IR and optical observations and data analysis, as

[1] www.bu.blazars/BEAM-ME.html

[2] http://polami.iaa.es/

[3] https://people.bu.edu/clemens/mimir/index.html

well as the host-galaxy modeling, are described in Appendix B.

4. IMPLICATIONS FOR PARTICLE ACCELERATION SCENARIOS

The spectral energy distribution of the synchrotron emission from 1ES 1959+650 typically peaks in the X-ray band ($\sim 0.1-100$ keV; Chang et al. 2019). It belongs to the category of high-frequency-peaked BL Lac-type blazars, a subclass that includes Mrk 501 and Mrk 421, which exhibit the highest X-ray fluxes (Perlman et al. 1996). In a leptonic-dominated emission scenario, the IR to X-ray emission from these objects is attributed to synchrotron radiation produced by electrons (and possibly positrons) in the jet's magnetic field. Synchrotron radiation is inherently polarized, with a degree of polarization of $\Pi \sim 70\%$ for electrons in a homogeneous magnetic field. After correcting for relativistic aberration, the polarization angle (ψ) at optically thin wavelengths is perpendicular to the average magnetic field direction projected onto the plane of the sky. In the case of BL Lac-type blazars, observations typically show polarization degrees of $\Pi \lesssim 20\%$ (Jorstad et al. 2005; Smith et al. 2007; Hovatta et al. 2016; Blinov et al. 2021).

There are two main reasons for the reduction in observed polarization. First, geometrical depolarization occurs when there is a random component in the magnetic field with varying orientations within the emitting region. This geometrical depolarization effect becomes more pronounced as the ratio of random to ordered magnetic field (B_r/B_0) increases (Ginzburg & Syrovatskii 1965). Second, temporal depolarization happens when the magnetic field direction changes over timescales shorter than integration time of the polarization measurement. The magnitude of this effect increases with the amplitude of unresolved changes in polarization angle (Di Gesu et al. 2022a; Zhang et al. 2022). This phenomenon was observed in *IXPE* observations of Mrk 421 (Di Gesu et al. 2023).

The degree of polarization in the X-ray band can be compared to that measured at optical frequencies during the same epoch. This polarization ratio Π_x/Π_O can be used as a diagnostic for potential differences in the magnetic field geometry and dynamics encountered by the populations of electrons responsible for the emission in each band. Previous *IXPE* observations of Mrk 501 and Mrk 421 have shown higher X-ray polarization compared to optical and radio frequencies (Liodakis et al. 2022; Di Gesu et al. 2022b), which can be explained by an energy-stratified particle distribution that would naturally arise in shock acceleration scenarios (e.g., Tavecchio et al. 2018).

In 2022 May 3-4, the ratio of X-ray to optical degree of polarization in 1ES 1959+650 was measured to be $\Pi_x/\Pi_O = 1.8 \pm 0.5$, lower than observed in Mrk 421 ($\Pi_x/\Pi_O \sim 5$; Di Gesu et al. 2022b) and comparable to Mrk 501 ($\Pi_x/\Pi_O \sim 2.5$; Liodakis et al. 2022). As in Mrk 501, the X-ray and optical polarization angles of 1ES 1959+650 were aligned (within 30°) with the jet direction, inferred to be $\phi \sim 150°$ from VLBA images (Piner et al. 2010; Weaver et al. 2022, Figure 4), indicating a magnetic field geometry consistent with a helical or toroidal configuration (Hovatta et al. 2012) or compression by a shock (Hughes et al. 1985).

In contrast, during the second *IXPE* exposure in 2022 June 9-12, the average optical polarization was $\Pi_O = 5.4\% \pm 1.1\%$, while the X-ray polarization was $\Pi_x < 5.1\%$ (Figure 3), suggesting $\Pi_x/\Pi_o \lesssim 1.0$. The optical polarization angle exhibited a rotation from $\psi_O \gtrsim 170°$ one day before June 9-12 to 103° during the *IXPE* exposure, returning to $\sim 160°$ five days after (Figure 2). Similar polarization angle excursions were observed in 2013-2016 (Blinov et al. 2021). IR observations also indicated a change in polarization angle during the second *IXPE* exposure. The X-ray flux exhibited smooth variations with a peak-to-valley amplitude of approximately 50% of the median X-ray flux (Figure 2).

Various single-zone models can explain the observed depolarization as geometrical. In shock acceleration scenarios, energy-dependent geometrical depolarization arises as electrons with decreasing energies occupy a larger volume, leading to a higher random magnetic field component and increased geometrical depolarization toward lower frequencies (Angelakis et al. 2016; Tavecchio et al. 2018; Liodakis et al. 2022). In magnetic reconnection scenarios, geometrical depolarization can occur due to the increasing range of magnetic field orientations as high-energy electrons move away from X-points where the highly-ordered magnetic field changes direction (Tchekhovskoy et al. 2009; Sironi & Spitkovsky 2014). However, a precise calculation of the X-ray versus optical polarization degree is not straightforward. The presence of a kink instability can create preferred locations for current sheets, and if the reconnecting fields are mainly toroidal (Zhang et al. 2022), the emitted radiation should exhibit a polarization angle roughly aligned with the jet axis.

Multi-zone models with turbulent magnetic field cells predict greater geometrical depolarization at optical frequencies than at X-ray energies (Marscher 2014). However, in such models it is the *mean* X-ray polarization that should exceed the *mean* optical polarization by a factor $\gtrsim 2$ (Marscher & Jorstad 2022). Temporal fluctuations of both, with a standard deviation equal to

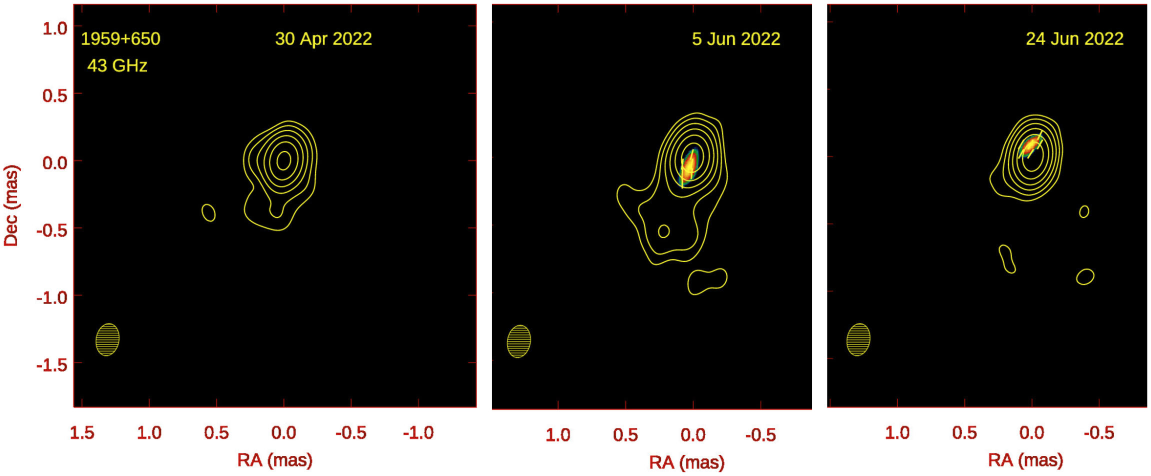

Figure 4. VLBA images of 1ES 1959+650 at 7 mm at three epochs contemporaneous with the *IXPE* observations. Contours: total intensity in factors of 2, starting at 2% of the peak intensity of (left to right) 0.16, 0.12, and 0.14 Jy per beam. Color coding: relative linearly polarized intensity, with maxima of (left to right) $<$ 4, 2.8, and 4.0 mJy per beam. Yellow line segments: electric-vector position angle of polarization. Cross-hatched ellipse in the lower left of each panel: FWHM of the elliptical restoring beam corresponding to the angular resolution along different directions. All positions are relative to the location of maximum intensity.

0.5 times the mean, are expected, so the Π_X/Π_O ratio should vary over time. Turbulence-based models also predict polarization angle swings that are not associated with changes in flux or polarization degree (Zhang et al. 2023).

5. CONCLUSIONS

In 2022 May 3-4, *IXPE* detected X-ray polarization from the BL Lac-type blazar 1ES 1959+650. The degree of polarization in the 2-8 keV band was measured to be $\Pi_x = 8.0 \pm 2.3$, with an electric-vector polarization position angle $\psi_x = 123^\circ \pm 8^\circ$. Bharathan et al. (2023) do not report a significant detection of X-ray polarization from this data set, possibly due to their use of a model-independent analysis that is less sensitive than the spectro-polarimetric analysis presented here. Our study constrains the degree of polarization during a second *IXPE* exposure in 2022 June 9-12 to $\Pi_x < 5.1\%$. Subsequent observations of 1ES 1959+650 with *IXPE* in October 2022 and August 2023 reveal increased X-ray polarization levels, reaching $\Pi_x = 12.5 \pm 0.7$ (Bharathan et al. 2023), compared to the levels from the earlier campaign reported here.

A time-resolved analysis of the second data set shows significant polarization during one of four 50 ks time bins, with polarization degree and angle compatible with the May 3-4 observation. Considering the measurement uncertainties, the hypothesis of a constant Π_x over the two observations can be only marginally rejected at 2.3σ confidence level.

During the 50-day period including the two *IXPE* observations, optical polarization measurements showed a range of $2.3\% \leq \Pi_O \leq 6.5\%$, with a median value of 3.9%. When comparing the degree of polarization between the X-ray and optical bands, a ratio of $\Pi_x/\Pi_O = 1.8 \pm 0.5$ was observed during May 3-4, while $\Pi_x/\Pi_o \lesssim 1.0$ was observed during June 9-12.

The amplitude of the galaxy-subtracted optical flux variability was 35% (peak to valley) during the campaign, while the X-ray flux changed by a factor of ~ 3. Although the optical and IR position angles of polarization varied significantly during the second *IXPE* pointing, the degree of polarization in these bands remained low, at around 4%. This suggests the presence of multiple magnetic field directions within the optical and IR emission regions, which could be a result of turbulence or magnetic reconnection events.

Recent observations of nearby high-frequency-peaked BL Lacs (Mrk 501 and Mrk 421, $z \sim 0.03$) at X-ray and optical frequencies have shown a higher degree of polarization in the X-ray band. This has been interpreted as evidence for an energy-stratified electron population dominating the observed radiative output of the jet (Liodakis et al. 2022; Di Gesu et al. 2022b). Similar results have been obtained with analogs of those objects at higher redshift (PG 1553+113, $z \sim 0.4$; 1ES 0229+200, $z = 0.140$; Middei et al. 2023a; Ehlert et al. 2023).

Our observations of 1ES 1959+650 represent the first time that X-ray polarization is detected from a high-frequency-peaked BL Lac without clearly exhibiting frequency dependence. The observed ratio $\Pi_x/\Pi_o \lesssim 1.0$ in 1ES 1959+650 during the second *IXPE* pointing is in apparent contradiction with a scenario where electrons emitting optical radiation occupy a larger volume with a more turbulent magnetic field compared to the higher energy electrons responsible for the X-ray emission. Nevertheless, the higher-amplitude flux variability in the X-ray band compared to that at optical frequencies suggests a more compact X-ray emitting region.

Temporal depolarization induced by turbulence in the X-ray emitting region could potentially explain occasions when the observed X-ray and optical polarization becomes $\Pi_X \approx \Pi_O$. If changes in polarization angle occur on timescales shorter than the 50 ks resolution of *IXPE* at the observed flux levels, the degree of polarization in the X-ray band will be suppressed. Optical observations, with integration times of $\lesssim 2$ ks, are less susceptible to temporal depolarization caused by slowly varying magnetic field configurations.

The change in optical polarization angle observed during the second *IXPE* pointing, in the absence of significant X-ray or optical flux variability, could be explained by multi-zone emission from turbulent plasma cells with typical dynamical timescales < 1 day. However, models based on turbulence alone do not predict alignment of the electric-vector polarization angle with the projected jet axis direction. During this campaign, we observed $\psi_x \approx \psi_o$ aligned within 30° of the projected jet direction, as measured with the VLBA. Models in which turbulent plasma crosses a shock have the potential to explain alignment with the jet as well as the time variability (Marscher 2014; Tavecchio et al. 2018; Tavecchio 2021).

A plausible alternative explanation for the lower degree of X-ray polarization measured in 1ES 1959+650 compared to Mrk 501 and Mrk 421 could be a minor contribution from the rising edge of the high-energy emission component of the spectral energy distribution to the observed 2-8 keV X-ray flux. This second emission component consists of Compton-scattered photons that are expected to have a very low degree of polarization (Krawczynski 2012). Thus, their presence in the *IXPE* data would weaken the measured degree of X-ray polarization in that band. Despite the absence of spectral curvature in the *Swift*-XRT and *XMM-Newton* spectral models, uncertainties might allow for a slight contribution from Compton-scattered emission at the highest energies. However, it is worth noting that no significant (inverted) spectral break, which would indicate a second spectral X-ray component, was indicated in the model fitting.

Given the time variability of the flux and polarization, further *IXPE* and multi-wavelength polarization and flux monitoring observations of 1ES 1959+650 are needed to probe the magnetic field geometry and the relationship between the emission regions at X-ray, optical, and IR wavelengths. During our campaign, the influence of geometrical and temporal depolarization cannot be fully distinguished. At X-ray flux levels of $F_{2-8\,\mathrm{keV}} = 10^{-10}\,\mathrm{erg\,cm^{-2}\,s^{-1}}$ and $\Pi_x \sim 8\%$, *IXPE* has the capability to detect changes in the polarization degree within approximately 50 ks. The sensitivity of *IXPE* scales as $MDP_{99} \propto (\texttt{exposure} \times F_{2-8\,\mathrm{keV}})^{-1/2}$, indicating that variations in X-ray polarization down to levels of $\Pi_x \lesssim 5\%$ could be resolved when the X-ray flux from 1ES 1959+650 is $F_{2-8\,\mathrm{keV}} \gtrsim 3 \times 10^{-10}\,\mathrm{erg\,cm^{-2}\,s^{-1}}$, or approximately twice as bright as the flux levels during the reported campaign. This capability has been demonstrated recently with the detection by *IXPE* of a $> 360°$ X-ray polarization angle rotation in Mrk 421 (Di Gesu et al. 2023).

Facilities: Calar Alto, IRAM-30m, *IXPE*, KANATA, NOT, Perkins, SNO, Skinakas, SMA, VLBA, *Swift*-XRT, *XMM-Newton*.

Software: astropy (Astropy Collaboration et al. 2013, 2018, 2022), Sherpa (Freeman et al. 2001), `Xspec` (Arnaud 1996), `ixpeobssim` (Baldini et al. 2022a,b), HEASoft (Heasarc 2014), SAS (Gabriel et al. 2004).

The authors thank Alex Chen for useful discussions on the expectations for a polarized flux arising from magnetic reconnection events. The Imaging X-ray Polarimetry Explorer (*IXPE*) is a joint US and Italian mission. The US contribution is supported by the National Aeronautics and Space Administration (NASA) and led and managed by its Marshall Space Flight Center (MSFC), with industry partner Ball Aerospace (contract NNM15AA18C). The Italian contribution is supported by the Italian Space Agency (Agenzia Spaziale Italiana, ASI) through contract ASI-OHBI-2017-12-I.0, agreements ASI-INAF-2017-12-H0 and ASI-INFN-2017.13-H0, and its Space Science Data Center (SSDC), and by the Istituto Nazionale di Astrofisica (INAF) and the Istituto Nazionale di Fisica Nucleare (INFN) in Italy. This research used data products provided by the *IXPE* Team (MSFC, SSDC, INAF, and INFN) and distributed with additional software tools by the High-Energy Astrophysics Science Archive Research Center (HEASARC), at NASA Goddard Space Flight Center (GSFC). We acknowledge financial support from ASI-INAF agreement n. 2022-14-HH.0. I. L. was supported by the NASA Postdoctoral Program at the Marshall Space Flight Center, administered by Oak Ridge Associated Universities under contract with NASA. The research at Boston University was supported in part by National Science Foundation grant AST-2108622 and by NASA Swift Guest Investigator grant 80NSSC22K0537, and Fermi Guest Investigator grants 80NSSC21K1917 and 80NSSC22K1571. This research has made use of data from the RoboPol program, a collaboration between Caltech, the University of Crete, IA-FORTH, IUCAA, the MPIfR, and the Nicolaus Copernicus University, which was conducted at Skinakas Observatory in Crete, Greece. The IAA-CSIC co-authors acknowledge financial support from the Spanish "Ministerio de Ciencia e Innovación" (MCIN/AEI/ 10.13039/501100011033) through the Center of Excellence Severo Ochoa award for the Instituto de Astrofísica de Andalucía-CSIC (CEX2021-001131-S), and through grants PID2019-107847RB-C44 and PID2022-139117NB-C44. Some of the data are based on observations collected at the Observatorio de Sierra Nevada, owned and operated by the Instituto de Astrofísica de Andalucía (IAA-CSIC). Further data are based on observations collected at the Centro Astronómico Hispano-Alemán(CAHA), operated jointly by Junta de Andalucía and Consejo Superior de Investigaciones Científicas (IAA-CSIC). The POLAMI observations were carried out at the IRAM 30m Telescope. IRAM is supported by INSU/CNRS (France), MPG (Germany) and IGN (Spain). The data in this study include observations made with the Nordic Optical Telescope, owned in collaboration by the University of Turku and Aarhus University, and operated jointly by Aarhus University, the University of Turku and the University of Oslo, representing Denmark, Finland and Norway, the University of Iceland and Stockholm University at the Observatorio del Roque de los Muchachos, La Palma, Spain, of the Instituto de Astrofisica de Canarias. The data presented here were obtained in part with ALFOSC, which is provided by the Instituto de Astrofísica de Andalucía (IAA) under a joint agreement with the University of Copenhagen and NOT. E. L. was supported by Academy of Finland projects 317636 and 320045. This study was based in part on observations conducted using the Perkins Telescope Observatory (PTO) in Arizona, USA, which is owned and operated by Boston University. We acknowledge funding to support our NOT observations from the Finnish Centre for Astronomy with ESO (FINCA), University of Turku, Finland (Academy of Finland grant nr 306531). Part of the French contribution is supported by the Scientific Research National Center (CNRS) and the French Spatial Agency (CNES). D.B., S.K., R.S., N. M., acknowledge support from the European Research Council (ERC) under the European Unions Horizon 2020 research and innovation programme under grant agreement No. 771282. CC acknowledges support by the European Research Council (ERC) under the HORIZON ERC Grants 2021 programme under grant agreement No. 101040021. The VLBA is an instrument of the National Radio Astronomy Observatory. The National Radio Astronomy Observatory is a facility of the National Science Foundation operated under cooperative agreement by Associated Universities, Inc. This work was supported by JST, the establishment of university fellowships towards the creation of science technology innovation, Grant Number JPMJFS2129. This work was supported by Japan Society for the Promotion of Science (JSPS) KAKENHI Grant Numbers JP21H01137. This work was also partially supported by the Optical and Near-Infrared Astronomy Inter-University Cooperation Program from the Ministry of Education, Culture, Sports, Science and Technology (MEXT) of Japan. We are grateful to the observation and operating members of the Kanata Telescope. The Submillimeter Array is a joint project between the Smithsonian Astrophysical Observatory and the Academia Sinica Institute of Astronomy and Astrophysics and is funded by the Smithsonian Institution and the Academia Sinica. Maunakea, the location of the SMA, is a culturally important site for the indigenous Hawaiian people; we are privileged to study the cosmos from its summit.

APPENDIX

A. X-RAY DATA REDUCTION

A.1. *IXPE*

Level 2 IXPE event files containing Stokes parameters calculated on an event-by-event basis were downloaded from the public `HEASARC` data repository. Data were further processed using `ixpeobssim v30.2.2` (Baldini et al. 2022a,b). Signal events were extracted using the `xpselect` tool from a 80″-radius circle centered on the sky location of 1ES 1959+650. Background photon counts were extracted from an annulus with inner radius of 140″ and outer radius of 200″ centered on the same location. This procedure was repeated for each of the three *IXPE* detector units (DU1–3, Weisskopf et al. 2022). Spectra were background-dominated at energies above 6 keV. Stokes I, Q, and U spectra in the 2-6 keV band were therefore extracted using `xpbin` without using event weights and binned to a minimum of 8 counts per bin. Spectropolarimetric analysis was performed using `Sherpa v4.14` (Burke et al. 2022), with custom spectro-polarimetry models equivalent to the `polconst` models found in `Xspec`. Normalization constants for detector units aFor June 9-12, the constant associated with *XMM-Newton* is 0.82 and that of *Swift*-XRT is 1.35, while those for detector units DU2 and DU3 are 0.97 and 0.92, all normalized to *IXPE* DU1. The wider spread in inter-calibration constants can be attributed to X-ray flux variability of 1ES 1959+650 during and after June 9-12.

A.2. *Swift-XRT*

Swift-XRT observations were performed both in photon counting and windowed timing mode. Files were processed using `xrtpipeline` packaged in `HEASoft v6.30` using the latest *Swift*-XRT calibration files. Signal events were extracted from a 60″-radius circle centered on 1ES 1959+650. Background photon counts were extracted from an annulus with inner radius of 150″ and outer radius of 280″. Spectra were binned to have at least 40 counts per energy bin and fit using `Xspec` (Arnaud 1996) to extract fluxes and spectral information.

A.3. *XMM-Newton*

XMM-Newton observations were performed with the PN camera in timing mode, using the thick filter to mitigate pile-up effects. EPAT plots clearly indicated the presence of pile-up in MOS cameras, rendering the MOS data unsuitable for analysis. Spectra were generated using version `20210317_1624-19.1.0` of the XMM-Newton Science Analysis Software (SAS) and the latest calibration products. To derive the spectrum of the source, a 27-pixel size box was employed, centered on the source itself. For background extraction, a region of the same size was selected from a blank area on the EPIC-pn CCD camera. To ensure accurate analysis, the resulting spectrum was appropriately rebinned to achieve a minimum of 30 counts per bin. Moderate pile-up was observed in the PN data below 1,keV, prompting the restriction of spectral analysis to the 1.0-10 keV energy range. After background subtraction, the net exposure in the PN camera is 1.39×10^4 s.

B. INFRARED/OPTICAL OBSERVATIONS AND DATA REDUCTION

B.1. *Infrared observations*

The IR observations were obtained with the MIMIR instrument at the 1.8m Perkins telescope in Flagstaff, Arizona. A detailed description of the camera and data reduction can be found in Clemens et al. (2012). One observation was the result of 6 dithering exposures of 10 s each at 16 positions of a half-wave plate, rotated in steps of 22.5° from 0° to 360°. Therefore, to determine polarization parameters at a given epoch, we collected 96 measurements of the source. We carried out 15 and 10 observations in H and K bands, respectively, from MJD 59736.5 to MJD 59748.5. To perform photometry, we have co-added all 96 exposures at a given epoch to construct a deep image. These deep images were also used to model the host galaxy of 1959+650 in H and K bands.

To make a model of the host galaxy, we used a photometric decomposition technique, which allows one to find an analytical model of an object and separate the light coming from its components. The distance to the object does not allow us to resolve it in great detail on our IR images, so in this work we adopted a rather simple model consisting of two components: a Sersic (Sérsic 1963; Sersic 1968) function to describe the host galaxy, and a point source for the active nucleus. We built the point-spread function (PSF) by averaging images of bright, isolated, and unsaturated stars, and fit the resulting image with a Moffat function (Moffat 1969) to produce a smooth image.

To run the decomposition, we used the IMFIT package (Erwin 2015). Our estimates of the host galaxy structural parameters are as follows: ellipticity $e = 0.31 \pm 0.05$, position angle $PA = 72.9 \pm 13.1°$, Sersic index $n = 1.55 \pm 0.5$, effective radius $r_e(K) = 2.53 \pm 0.46''$, $r_e(H) = 2.84 \pm 0.35''$, effective surface brightness $\mu_e(K) = 16.98 \pm 0.39''$, and $\mu_e(H) = 17.65 \pm 0.27''$ mag per square arcsecond. The rather large uncertainties, especially in the Sersic index value, are attributed to poor resolution of the object: the observed object effective radius is close to the PSF FWHM, which results in a degradation of the decomposition quality (Trujillo et al. 2001). We have employed the model parameters to estimate contributions of the host galaxy of 1959+650 within an aperture of diameter 5$''$ that are equal to 14.28 ± 0.09 mag and 13.71 ± 0.05 mag in H and K bands, respectively.

B.2. *Optical Observations*

The optical R-band observations were performed at the Calar Alto observatory, KANATA telescope, the Nordic Optical Telescope (NOT) using the Alhambra Faint Object Spectrograph and Camera (ALFOSC), the Sierra Nevada observatory, and at the Skinakas observatory using the RoboPol polarimeter. The Calar Alto and SNO observations were obtained on 2022 June 6, 10, and 17 (MJD 59737.1, 59740.9, 59741.0, and 59747.8), and analyzed using standard photo-polarimetric procedures. The KANATA observations were obtained on 2022 May 3 (MJD 59702.0) using the Hiroshima Optical and Near-InfraRed camera (HONIR, Akitaya et al. 2014; Kawabata et al. 1999), and analyzed using standard procedures. The NOT observations were obtained on 2022 May 4 (MJD 59703.1) and 2022 June 7 (MJD 59737.1). The data were analyzed using unpolarized and polarized standard stars for calibration, following the standard photometric procedures included in the Tuorla Observatory pipeline (Hovatta et al. 2016; Nilsson et al. 2018). The RoboPol polarimeter is a novel 4-channel polarimeter that simultaneously measures Π_O and ψ_O with a single exposure (Ramaprakash et al. 2019). Details of the analysis pipeline and data reduction procedures can be found in Panopoulou et al. (2015) and Blinov et al. (2021).

All of the optical observations were corrected for the depolarization effect of unpolarized host-galaxy contribution to the emission following Nilsson et al. (2007). A more detailed description of the analysis procedures from the different observatories can be found in Liodakis et al. (2022); Di Gesu et al. (2022b); Middei et al. (2023b).

REFERENCES

Agudo, I., Thum, C., Ramakrishnan, V., et al. 2018a, MNRAS, 473, 1850, doi: 10.1093/mnras/stx2437

Agudo, I., Thum, C., Molina, S. N., et al. 2018b, MNRAS, 474, 1427, doi: 10.1093/mnras/stx2435

Akitaya, H., Moritani, Y., Ui, T., et al. 2014, in Society of Photo-Optical Instrumentation Engineers (SPIE) Conference Series, Vol. 9147, Ground-based and Airborne Instrumentation for Astronomy V, ed. S. K. Ramsay, I. S. McLean, & H. Takami, 91474O, doi: 10.1117/12.2054577

Aliu, E., Archambault, S., Arlen, T., et al. 2013, ApJ, 775, 3, doi: 10.1088/0004-637X/775/1/3

—. 2014, ApJ, 797, 89, doi: 10.1088/0004-637X/797/2/89

Angel, J. R. P., & Stockman, H. S. 1980, ARA&A, 18, 321, doi: 10.1146/annurev.aa.18.090180.001541

Angelakis, E., Hovatta, T., Blinov, D., et al. 2016, MNRAS, 463, 3365, doi: 10.1093/mnras/stw2217

Arnaud, K. A. 1996, in Astronomical Society of the Pacific Conference Series, Vol. 101, Astronomical Data Analysis Software and Systems V, ed. G. H. Jacoby & J. Barnes, 17

Astropy Collaboration, Robitaille, T. P., Tollerud, E. J., et al. 2013, A&A, 558, A33, doi: 10.1051/0004-6361/201322068

Astropy Collaboration, Price-Whelan, A. M., Sipőcz, B. M., et al. 2018, AJ, 156, 123, doi: 10.3847/1538-3881/aabc4f

Astropy Collaboration, Price-Whelan, A. M., Lim, P. L., et al. 2022, ApJ, 935, 167, doi: 10.3847/1538-4357/ac7c74

Baldini, L., Bucciantini, N., Lalla, N. D., et al. 2022a, SoftwareX, 19, 101194, doi: 10.1016/j.softx.2022.101194

—. 2022b, ixpeobssim: Imaging X-ray Polarimetry Explorer simulator and analyzer, Astrophysics Source Code Library, record ascl:2210.020. http://ascl.net/2210.020

Begelman, M. C., Blandford, R. D., & Rees, M. J. 1984, Reviews of Modern Physics, 56, 255, doi: 10.1103/RevModPhys.56.255

Bharathan, A. M., Stalin, C. S., Chatterjee, R., et al. 2023, arXiv e-prints, arXiv:2311.01745, doi: 10.48550/arXiv.2311.01745

Blandford, R., Meier, D., & Readhead, A. 2019, ARA&A, 57, 467, doi: 10.1146/annurev-astro-081817-051948

Blandford, R. D., & Ostriker, J. P. 1978, ApJL, 221, L29, doi: 10.1086/182658

Blandford, R. D., & Znajek, R. L. 1977, MNRAS, 179, 433, doi: 10.1093/mnras/179.3.433

Blinov, D., Kiehlmann, S., Pavlidou, V., et al. 2021, MNRAS, 501, 3715, doi: 10.1093/mnras/staa3777

Bodo, G., Tavecchio, F., & Sironi, L. 2021, MNRAS, 501, 2836, doi: 10.1093/mnras/staa3620

Burke, D., Laurino, O., Günther, H. M., et al. 2022, sherpa/sherpa: Sherpa 4.15.0, 4.15.0, Zenodo, doi: 10.5281/zenodo.7186379

Burrows, D. N., Hill, J. E., Nousek, J. A., et al. 2005, SSRv, 120, 165, doi: 10.1007/s11214-005-5097-2

Chang, Y. L., Arsioli, B., Giommi, P., Padovani, P., & Brandt, C. H. 2019, A&A, 632, A77, doi: 10.1051/0004-6361/201834526

Clemens, D. P., Pinnick, A. F., & Pavel, M. D. 2012, ApJS, 200, 20, doi: 10.1088/0067-0049/200/2/20

de Vaucouleurs, G., de Vaucouleurs, A., Corwin, Herold G., J., et al. 1991, Third Reference Catalogue of Bright Galaxies

Dermer, C. D., Miller, J. A., & Li, H. 1996, ApJ, 456, 106, doi: 10.1086/176631

Di Gesu, L., Tavecchio, F., Donnarumma, I., et al. 2022a, A&A, 662, A83, doi: 10.1051/0004-6361/202243168

Di Gesu, L., Donnarumma, I., Tavecchio, F., et al. 2022b, ApJL, 938, L7, doi: 10.3847/2041-8213/ac913a

Di Gesu, L., Marshall, H. L., Ehlert, S. R., et al. 2023, Nature Astronomy, 7, 1245, doi: 10.1038/s41550-023-02032-7

Ehlert, S. R., Liodakis, I., Middei, R., et al. 2023, ApJ, 959, 61, doi: 10.3847/1538-4357/ad05c4

Erwin, P. 2015, ApJ, 799, 226, doi: 10.1088/0004-637X/799/2/226

Falcke, H., Körding, E., & Markoff, S. 2004, A&A, 414, 895, doi: 10.1051/0004-6361:20031683

Freeman, P., Doe, S., & Siemiginowska, A. 2001, in Society of Photo-Optical Instrumentation Engineers (SPIE) Conference Series, Vol. 4477, Astronomical Data Analysis, ed. J.-L. Starck & F. D. Murtagh, 76–87, doi: 10.1117/12.447161

Gabriel, C., Denby, M., Fyfe, D. J., et al. 2004, in Astronomical Society of the Pacific Conference Series, Vol. 314, Astronomical Data Analysis Software and Systems (ADASS) XIII, ed. F. Ochsenbein, M. G. Allen, & D. Egret, 759

Ginzburg, V. L., & Syrovatskii, S. I. 1965, ARA&A, 3, 297, doi: 10.1146/annurev.aa.03.090165.001501

Giommi, P., Polenta, G., Lähteenmäki, A., et al. 2012, A&A, 541, A160, doi: 10.1051/0004-6361/201117825

Heasarc. 2014, HEAsoft: Unified Release of FTOOLS and XANADU, Astrophysics Source Code Library, record ascl:1408.004. http://ascl.net/1408.004

HI4PI Collaboration, Ben Bekhti, N., Flöer, L., et al. 2016, A&A, 594, A116, doi: 10.1051/0004-6361/201629178

Holder, J., Bond, I. H., Boyle, P. J., et al. 2003, ApJL, 583, L9, doi: 10.1086/367816

Hovatta, T., Lister, M. L., Aller, M. F., et al. 2012, AJ, 144, 105, doi: 10.1088/0004-6256/144/4/105

Hovatta, T., Lindfors, E., Blinov, D., et al. 2016, A&A, 596, A78, doi: 10.1051/0004-6361/201628974

Hughes, P. A., Aller, H. D., & Aller, M. F. 1985, ApJ, 298, 301, doi: 10.1086/163611

Hughes, P. A., & Bregman, J. N., eds. 2006, American Institute of Physics Conference Series, Vol. 856, Relativistic Jets: The Common Physics of AGN, Microquasars, and Gamma-Ray Bursts

Jorstad, S. G., Marscher, A. P., Lister, M. L., et al. 2005, AJ, 130, 1418, doi: 10.1086/444593

Jorstad, S. G., Marscher, A. P., Morozova, D. A., et al. 2017, ApJ, 846, 98, doi: 10.3847/1538-4357/aa8407

Kagan, D., Sironi, L., Cerutti, B., & Giannios, D. 2015, SSRv, 191, 545, doi: 10.1007/s11214-014-0132-9

Kapanadze, B., Romano, P., Vercellone, S., Kapanadze, S., & Kharshiladze, G. 2014, in Proceedings of Swift: 10 Years of Discovery (SWIFT 10, 142, doi: 10.22323/1.233.0142

Katarzyński, K., Ghisellini, G., Mastichiadis, A., Tavecchio, F., & Maraschi, L. 2006, A&A, 453, 47, doi: 10.1051/0004-6361:20054176

Kawabata, K. S., Okazaki, A., Akitaya, H., et al. 1999, PASP, 111, 898, doi: 10.1086/316387

Kirk, J. G., Duffy, P., & Gallant, Y. A. 1996, A&A, 314, 1010, doi: 10.48550/arXiv.astro-ph/9604056

Krawczynski, H. 2012, ApJ, 744, 30, doi: 10.1088/0004-637X/744/1/30

Krawczynski, H., Hughes, S. B., Horan, D., et al. 2004, ApJ, 601, 151, doi: 10.1086/380393

Liodakis, I., Peirson, A. L., & Romani, R. W. 2019, ApJ, 880, 29, doi: 10.3847/1538-4357/ab2719

Liodakis, I., Marscher, A. P., Agudo, I., et al. 2022, Nature, 611, 677, doi: 10.1038/s41586-022-05338-0

Lyubarsky, Y. E. 2010, Monthly Notices of the Royal Astronomical Society, 402, 353, doi: 10.1111/j.1365-2966.2009.15877.x

Madsen, K. K., Beardmore, A. P., Forster, K., et al. 2017, AJ, 153, 2, doi: 10.3847/1538-3881/153/1/2

Marrone, D. P., & Rao, R. 2008, in Proc. SPIE, Vol. 7020, Millimeter and Submillimeter Detectors and Instrumentation for Astronomy IV, ed. W. D. Duncan, W. S. Holland, S. Withington, & J. Zmuidzinas, 70202B, doi: 10.1117/12.788677

Marscher, A. P. 2014, ApJ, 780, 87, doi: 10.1088/0004-637X/780/1/87

Marscher, A. P., & Jorstad, S. G. 2021, Galaxies, 9, 27, doi: 10.3390/galaxies9020027

—. 2022, Universe, 8, 644, doi: 10.3390/universe8120644

Middei, R., Perri, M., Puccetti, S., et al. 2023a, ApJL, 953, L28, doi: 10.3847/2041-8213/acec3e

Middei, R., Liodakis, I., Perri, M., et al. 2023b, ApJL, 942, L10, doi: 10.3847/2041-8213/aca281

Moffat, A. F. J. 1969, A&A, 3, 455

Nilsson, K., Pasanen, M., Takalo, L. O., et al. 2007, A&A, 475, 199, doi: 10.1051/0004-6361:20077624

Nilsson, K., Lindfors, E., Takalo, L. O., et al. 2018, A&A, 620, A185, doi: 10.1051/0004-6361/201833621

Nishikawa, K. I., Hardee, P., Richardson, G., et al. 2003, ApJ, 595, 555, doi: 10.1086/377260

Panopoulou, G., Tassis, K., Blinov, D., et al. 2015, MNRAS, 452, 715, doi: 10.1093/mnras/stv1301

Perlman, E. S., Stocke, J. T., Schachter, J. F., et al. 1996, ApJS, 104, 251, doi: 10.1086/192300

Piner, B. G., Pant, N., & Edwards, P. G. 2010, ApJ, 723, 1150, doi: 10.1088/0004-637X/723/2/1150

Primiani, R. A., Young, K. H., Young, A., et al. 2016, Journal of Astronomical Instrumentation, 5, 1641006, doi: 10.1142/S2251171716410063

Ramaprakash, A. N., Rajarshi, C. V., Das, H. K., et al. 2019, MNRAS, 485, 2355, doi: 10.1093/mnras/stz557

Romanova, M. M., & Lovelace, R. V. E. 1992, A&A, 262, 26

Rybicki, G. B., & Lightman, A. P. 1979, Radiative processes in astrophysics

Sérsic, J. L. 1963, Boletin de la Asociacion Argentina de Astronomia La Plata Argentina, 6, 41

Sersic, J. L. 1968, Atlas de Galaxias Australes

Sironi, L., Keshet, U., & Lemoine, M. 2015a, SSRv, 191, 519, doi: 10.1007/s11214-015-0181-8

Sironi, L., Petropoulou, M., & Giannios, D. 2015b, MNRAS, 450, 183, doi: 10.1093/mnras/stv641

Sironi, L., & Spitkovsky, A. 2014, ApJL, 783, L21, doi: 10.1088/2041-8205/783/1/L21

Smith, P. S., Williams, G. G., Schmidt, G. D., Diamond-Stanic, A. M., & Means, D. L. 2007, ApJ, 663, 118, doi: 10.1086/517992

Stroh, M. C., & Falcone, A. D. 2013, ApJS, 207, 28, doi: 10.1088/0067-0049/207/2/28

Strüder, L., Briel, U., Dennerl, K., et al. 2001, A&A, 365, L18, doi: 10.1051/0004-6361:20000066

Tagliaferri, G., Foschini, L., Ghisellini, G., et al. 2008, ApJ, 679, 1029, doi: 10.1086/586731

Tavecchio, F. 2021, Galaxies, 9, 37, doi: 10.3390/galaxies9020037

Tavecchio, F., Landoni, M., Sironi, L., & Coppi, P. 2018, MNRAS, 480, 2872, doi: 10.1093/mnras/sty1491

—. 2020, MNRAS, 498, 599, doi: 10.1093/mnras/staa2457

Tchekhovskoy, A., McKinney, J. C., & Narayan, R. 2009, ApJ, 699, 1789, doi: 10.1088/0004-637X/699/2/1789

Thum, C., Agudo, I., Molina, S. N., et al. 2018, MNRAS, 473, 2506, doi: 10.1093/mnras/stx2436

Trujillo, I., Aguerri, J. A. L., Cepa, J., & Gutiérrez, C. M. 2001, MNRAS, 328, 977, doi: 10.1046/j.1365-8711.2001.04937.x

Urry, C. M., & Padovani, P. 1995, PASP, 107, 803, doi: 10.1086/133630

Vlahakis, N., & Königl, A. 2004, ApJ, 605, 656, doi: 10.1086/382670

Weaver, Z. R., Jorstad, S. G., Marscher, A. P., et al. 2022, ApJS, 260, 12, doi: 10.3847/1538-4365/ac589c

Weisskopf, M. C., Soffitta, P., Baldini, L., et al. 2022, Journal of Astronomical Telescopes, Instruments, and Systems, 8, 026002, doi: 10.1117/1.JATIS.8.2.026002

Werner, G. R., Uzdensky, D. A., Begelman, M. C., Cerutti, B., & Nalewajko, K. 2018, MNRAS, 473, 4840, doi: 10.1093/mnras/stx2530

Zhang, H., Fang, K., Li, H., et al. 2019, ApJ, 876, 109, doi: 10.3847/1538-4357/ab158d

Zhang, H., Li, X., Giannios, D., et al. 2022, ApJ, 924, 90, doi: 10.3847/1538-4357/ac3669

Zhang, H., Marscher, A. P., Guo, F., et al. 2023, ApJ, 949, 71, doi: 10.3847/1538-4357/acc657